Mode-selective excitation of hydrogen atoms on a Si surface: Non-Markovian and Markovian treatment of infrared laser driven dissipative quantum dynamics

Guennadij K. Paramonov
B.I. Stepanov Institute of Physics, National Academy of Sciences of Belarus, Independence ave. 70, 220602 Minsk, Belarus

Stephanie Beyvers, Ivan Andrianov, and Peter Saalfrank*
Institut für Chemie, Universität Potsdam, Karl-Liebknecht-Str. 24-25, D-14476 Potsdam-Golm, Germany
(Received 14 September 2006; revised manuscript received 16 November 2006; published 8 January 2007)

Mode-selective excitation of adsorbates by shaped infrared laser pulses is investigated here theoretically, for the example of a H atom on a hydrogen-covered Si(100)-2×1 surface. The mode-selective excitation is perturbed by the intermode coupling within the system (bending and stretching modes) and by system-bath coupling to substrate phonons. Using a force-field based model, vibration-phonon coupling was found and predicted to lead to vibrational relaxation of the H-Si stretching mode on a ns timescale, and of the Si-Si-H bending mode on a ps timescale [I. Andrianov and P. Saalfrank, J. Chem. Phys. **124**, 034710 (2006)]. To address the question as to whether in such a dissipative situation mode-selective control of adsorbate vibrational dynamics is still possible, a system-bath ansatz is used to derive an open-system density matrix theory in which the H vibrations are driven either by $\sin^2$, or by freely optimized infrared ps laser pulses. Both for the Si-H stretching and Si-Si-H bending vibrations mode-selective excitation is predicted to be possible. It is also found that the Markov approximation works well in most of the applications, and that simple $\sin^2$ are nearly as effective as pulses which were freely optimized by optimal control theory.

DOI: 10.1103/PhysRevB.75.045405 PACS number(s): 68.43.Pq, 82.50.Nd

I. INTRODUCTION

Hydrogen-covered silicon surfaces are interesting microlabs for a variety of phenomena in fundamental and applied surface science. For example, for H-covered Si(100) and/or Si(111) surfaces the vibrational lifetime of the Si-H stretch mode, which is governed by vibration-phonon coupling, has been measured at various temperatures.[1] Accordingly, the lifetime of the $v=1$ stretching vibration in H:Si(100)-2×1, where each of the Si atoms of the Si_2 dimers of the reconstructed Si(100)-2×1 surface carries one H atom, is about 1.2 ns at $T=300$ K.[1] This figure increases to several ns with decreasing temperature.[1] The H:Si(111)-1×1 surface behaves similarly. Large isotope effects have been observed when H is replaced by D: For D:Si(100)-2×1, the lifetime drops to a few hundred ps. This is due to the smaller Si-D frequency, which is still larger than the Debye frequency of the Si surface but the frequency mismatch between the adsorbate and the substrate vibrations is already smaller. Similarly, for the bending vibration of H on Si(100)-2×1 along the Si-Si-H bending angle, a vibrational relaxation time in the order of a ps has been predicted theoretically.[2] The Si-Si-H bending vibration has a frequency close to the Debye frequency of the solid, and was predicted to relax by a two-phonon process.[2] Similar short lifetimes were predicted for the C-H stretching modes of H-terminated diamond surfaces.[3,4] For example, for H:C(100) a vibrational lifetime of 0.8 ps was calculated, which is due to a 1:2 resonance.[4]

Vibrational relaxation greatly affects surface reactions, when enforced by external stimuli. For H:Si(100)-2×1, a number of reactions were enforced with electrons or holes [from a scanning tunneling microscope (STM)], or a laser. These inlcude the desorption of H atoms[5–8] and the lateral motion ("switching") of H atoms from one dangling bond site of a Si dimer to a neighboring one.[9,10] The rate for STM-driven desorption of hydrogen atoms from H:Si(100)-2×1 in the "below-threshold" regime[6] (low voltages) is in established dynamical models inversely proportional to the lifetime of the Si-H stretching mode.[11] In this case the tunneling electrons drive the adsorbate-surface up along the vibrational ladder, a process which is perturbed by downward transitions due to vibration-phonon coupling. Similarly, vibrational relaxation is also important for femtosecond laser induced reactions at metal surfaces.[12,13]

Some of the above reactions proceed by vibrational ladder climbing in the ground state, however, under explicit participation of higher-lying electronically excited states. The interesting question arises as to whether the vibrational excitation could also be directly enforced by infrared (IR) light. In particular one would like to *selectively* excite a bond, e.g., to break it. A slightly less ambitious application of bond-selective excitation is *vibrationally mediated chemistry*. An example is the well-known IR+UV strategy, where IR photons selectively excite a bond, which then breaks with enhanced probability after electronic excitation by UV/vis light.[14] An analogous strategy was suggested in surface science to enhance photoreaction (in particular photodesorption) cross sections.[10,15–18]

Some time ago IR laser induced photodesorption of NH_3 from Cu(100) was observed experimentally, however, with frequencies that excite the N-H stretching mode of about 3400 cm^{-1}.[19] It was argued that the desorption mechanism is thermal. Accordingly, the N-H bond serves as an antenna that directs radiation energy via surface phonons to the molecule-surface bond, and breaks it. Unfortunately, the process is nonselective because also coadsorbed ND_3 desorbs when NH_3 is excited. Only recently the goal was achieved to *selectively* excite and break an adsorbate-surface bond by IR

photons without thermalization. The example system was a Si(111) surface, with H and D atoms coadsorbed on it. After exciting the Si-H bond with IR radiation that was resonant with the Si-H vibration, the desorption of H_2 (not D_2) was observed.[20] This may well be the first example of bond-selective excitation in a polyatomic system.[21] The reason why bond-selective IR excitation is so difficult to achieve in polyatomic molecules or in condensed phases is the rapid quenching of the excitation due to coupling of the vibration of interest to a multitude of other modes.

The goal of this paper is to address the question to which extent *bond-* and perhaps even *state*-selective IR excitation of selected adsorbate vibrations is possible. We are specifically considering the H:Si(100)-2×1 system, for which we can build on previous experience.[2,22,23] The vibration-phonon coupling is treated within a system-bath model and open-system density matrix theory. Further issues to be addressed are non-Markovian[16,24] vs Markovian[2] behavior, and the performance of various strategies to create optimal IR pulses—either by choosing a fixed shape function, or by free optimization using optimal control theory.[25–28]

The paper is organized as follows. In Sec. II the H:Si(100)-2×1 system is introduced, along with a system-bath model. Equations of motion derived from non-Markovian (Sec. III A) and Markovian (Sec. III B) open-system density matrix theories are summarized in Sec. III A, brief account of pulse generation and analysis is given in Sec. III C. In Sec. IV results on the (field-free) vibrational relaxation (Sec. IV A), and the mode- and state-selective excitation of selected adsorbate vibrations by shaped IR laser pulses (Sec. IV B) will be presented and discussed. Section V summarizes this work and addresses possible future directions.

II. MODEL

The model Hamiltonian characterizing the combined total system, a H atom adsorbed on a Si dimer of a reconstructed, H-covered Si(100):2×1 surface and being excited by the laser field, can be written in the form

$$\hat{H} = \hat{H}_S + \hat{H}_{SF} + \hat{H}_{SB} + \hat{H}_B, \tag{1}$$

where $\hat{H}_S$ is the system Hamiltonian, $\hat{H}_{SF}$ and $\hat{H}_{SB}$ represent the system-field and the system-bath coupling, respectively, and $\hat{H}_B$ is the bath Hamiltonian.

The system Hamiltonian in polar coordinates reads

$$\hat{H}_S(r,\phi) = -\frac{\hbar^2}{2m}\frac{\partial^2}{\partial r^2} - \frac{\hbar^2}{2mr^2}\frac{\partial^2}{\partial \phi^2} + V(r,\phi), \tag{2}$$

where m is the mass of the hydrogen atom, and r and ϕ represent the H-Si stretching mode (the Si-H distance), and the Si-Si-H bending motion coordinates, respectively, of an H atom adsorbed on the H:Si(100)-2×1 surface. $V(r,\phi)$ is the two-dimensional (2D) potential energy surface of the adsorbed H atom, for which we take the same model form

$$V(r,\phi) = D(e^{-2\alpha(r-r_0)} - 2e^{-\alpha(r-r_0)}) + D + \frac{k}{2}e^{-\beta(r-r_0)^2}(\phi-\phi_0)^2, \tag{3}$$

as in Ref. 2. Here $D=3.4$ eV is the H binding energy, the equilibrium position of H on a Si dimer is $r_0=2.84$ a_0, $\phi_0=112.6°$, and other parameters are as defined in Ref. 2. The potential function (3) supports bound vibrational states $\psi_v(r,\phi)$, the lowest of which can be characterized according to their stretch and bending quantum numbers, i.e., $v=(v_r,v_\phi)$. The fundamental frequencies of the bending and stretching modes, obtained by diagonalization of the system Hamiltonian with the sinc-function discrete-variable-representation method,[29] are $\omega_r=2037$ cm^{-1} and $\omega_\phi=637$ cm^{-1}, in reasonable agreement with experiment.[1]

The laser field is assumed to be linearly polarized perpendicular to the Si-dimers of the Si(100)-2×1 surface, which we denote the z direction. Its interaction with the system is described within the semiclassical electric dipole approximation by the interaction Hamiltonian

$$\hat{H}_{SF}(r,\phi,t) = -\mu_z(r,\phi)E_z(t), \tag{4}$$

where $E_z(t)$ is the laser electric field, and $\mu_z(r,\phi)$ is the z component of the dipole moment. To estimate the latter, B3LYP/6–31G** (Ref. 30) calculations with GAUSSIAN (Ref. 31) were carried out for a small Si_6H_2 cluster, mimicking a fully H-covered Si_2 dimer of the 2×1 reconstructed Si(100) surface, plus its nearest four Si atoms of the second layer of the Si lattice. In the calculation, r and ϕ for one of the H atoms were varied while all other atoms were kept fixed at positions which were optimized, using a bond-order forcefield, for a 180-atom cluster in Ref. 2 (see below). The numerically derived dipole function was then parametrized as

$$\mu_z(r,\phi) = A_0 + A_1(r-r_0)e^{-A_2(r-r_0)} + A_3(\phi-\phi_0) \tag{5}$$

with parameters $A_0=0.4001$ ea_0, $A_1=-1.2587$ e, $A_2=0.3175$ a_0^{-1}, and $A_3=-0.4734$ ea_0/rad (1 rad=57.3°). Equation (5) holds only for small values of $\phi-\phi_0$. Vibrational transition dipole matrix elements were calculated as

$$\mu_{v'v} = \langle \psi_{v'} | \mu_z(r,\phi) | \psi_v \rangle. \tag{6}$$

The bath Hamiltonian, based on the normal-mode analysis of large clusters $Si_nH_m^2$, reads:

$$\hat{H}_B(\{q_i\}) = \sum_{i=1}^{N_B}\left(-\frac{\hbar^2}{2M_i}\frac{\partial^2}{\partial q_i^2} + \frac{1}{2}M_i\omega_i^2 q_i^2\right), \tag{7}$$

where M_i and ω_i are the masses and frequencies of the normal modes of the cluster. To obtain the normal modes, use is made of a semi-empirical bond order potential by Dyson and Smith.[32,33] All results below are for a hydrogenated silicon cluster consisting of $N_{at}=180$ atoms (36 H and 144 Si atoms),[2] giving a total of $N_B=3N_{at}-6=534$ normal modes. The bath modes extend up to a calculated Debye frequency of 579 cm^{-1}, in good accord with other sources,[11] and lower than the two system frequencies ω_r and ω_ϕ of above.

TABLE I. Quantum numbers $v=(v_r,v_\phi)$, energies (relative to the ground state), and vibrational lifetimes τ_v $(T=0)$ of the lowest seven vibrational eigenstates $|v\rangle$, along with the downward decay rates $\Gamma_{v'\to v}$ at $T=0$ K (lower left half of the table, in ps^{-1}), and the dipole matrix elements, $|\mu_{v'v}|$ (in atomic units ea_0) in the upper right half.

v	0	1	2	3	4	5	6
(v_r,v_ϕ)	(0,0)	(0,1)	(0,2)	(0,3)	(1,0)	(0,4)	(1,1)
ω_{v0} (cm^{-1})	0	637	1271	1903	2037	2532	2661
τ_v (ps)	—	1.35	0.69	0.48	2130	0.37	1.45
v'							
0	—	5.06×10^{-2}	8.52×10^{-3}	1.61×10^{-4}	2.06×10^{-1}	7.64×10^{-5}	1.50×10^{-3}
1	0.7383	—	7.13×10^{-2}	1.48×10^{-2}	3.32×10^{-3}	3.23×10^{-4}	2.05×10^{-1}
2	0.	1.4426	—	8.71×10^{-2}	1.17×10^{-3}	2.10×10^{-2}	4.74×10^{-3}
3	0.	0.	2.1034	—	4.62×10^{-5}	1.00×10^{-1}	2.05×10^{-3}
4	0.	0.	4.70×10^{-4}	9.80×10^{-8}	—	5.16×10^{-6}	5.04×10^{-2}
5	0.	0.	0.	2.7154	4.69×10^{-6}	—	9.32×10^{-5}
6	0.	0.	0.	1.23×10^{-3}	0.6895	3.72×10^{-7}	—

By a truncated Taylor expansion of the same semiempirical force field the system-bath interaction Hamiltonian has been determined as

$$\hat{H}_{SB}(r,\phi,\{q_i\}) = \sum_i^{N_B} \lambda_i(r,\phi)q_i + \frac{1}{2}\sum_i^{N_B}\sum_j^{N_B} \Lambda_{ij}(r,\phi)q_iq_j. \quad (8)$$

The system-bath Hamiltonian (8) takes into account both one- and two-phonon transitions in the bath, the latter being necessary to efficiently couple the high-frequency system modes, to the low-frequency bath modes.[2] The one- and two-phonon coupling functions λ_i and Λ_{ij} are nonlinear in the system coordinates, see Ref. 2 for details.

Based on this model and using Fermi's Golden Rule, transition rates $\Gamma_{v'\to v}$ between system states $|v'\rangle$ and $|v\rangle$ due to one- and two-phonon transitions, were determined in Ref. 2. Also, vibrational lifetimes τ_v of system eigenstates were calculated by summing appropriately over all contributing transition rates. For $T=0$ K, it was found that $\tau_1=\tau_{(0,1)}=1.35$ ps for the bending mode (first index: stretch; second index: bending) and $\tau_4=\tau_{(1,0)}=2.13$ ns. Downward and upward rates are related by detailed balance,

$$\Gamma_{v\to v'} = \Gamma_{v'\to v}e^{-\hbar\omega_{vv'}/k_BT} \quad (9)$$

giving $\tau_{(1,0)}\approx 1.5$ ns at 300 K.[2] The calculated lifetime of the stretching mode is in good agreement with experiment,[1] while the lifetime of the bending vibration, being three orders of magnitude shorter, has so far not been measured according to our knowledge. Its order of magnitude, however, is supported by a recent nonperturbative study.[23]

For completeness, we show in Table I the quantum numbers, energies (relative to the ground state), and vibrational lifetimes τ_v $(T=0)$ of the lowest seven system eigenstates $|v\rangle$ $(v=0,\ldots,6)$, along with the downward decay rates $\Gamma_{v'\to v}$ and the dipole matrix elements, $|\mu_{v'v}|$. In the dynamics calculations below, up to the lowest 50 vibrational states will be considered.

III. EQUATIONS OF MOTION AND TECHNIQUES

In the following, we will use a reduced density matrix description for the laser-driven vibrational system dynamics. Two variants will be used; one, in which memory is included (non-Markovian theory) and one in which the Markov approximation is made.

A. Non-Markovian theory

In this subsection, the interaction picture will be used. It is suitable to start with the equation of motion for the combined total system descibed by the Hamiltonian (1). The density operator characterizing the total system in the interaction picture is denoted by $\hat{\sigma}^I(t)$. Its time evolution is governed by the Liouville equation, see, e.g., Ref. 34,

$$\frac{\partial\hat{\sigma}^I(t)}{\partial t} = \frac{i}{\hbar}E_z(t)[\mu_z^I(r,\phi,t),\hat{\sigma}^I(t)] - \frac{i}{\hbar}[\hat{H}_{SB}^I(r,\phi,\{q_i\},t),\sigma^I(t)]. \quad (10)$$

The density operator $\sigma^I(t)$ and the operators of Eq. (10) in the interaction picture are related to the Schrödinger picture as follows:

$$\hat{\sigma}^I(t) = e^{i(\hat{H}_S+\hat{H}_B)t/\hbar}\hat{\sigma}(t)e^{-i(\hat{H}_S+\hat{H}_B)t/\hbar}, \quad (11)$$

$$B^I(r,\phi,t) = e^{i\hat{H}_St/\hbar}B(r,\phi)e^{-i\hat{H}_St/\hbar} \quad (\text{with } B=\mu_z,\ \lambda_i,\ \text{or } \Lambda_{ij}), \quad (12)$$

$$q_i^I(t) = e^{i\hat{H}_Bt/\hbar}q_ie^{-i\hat{H}_Bt/\hbar}. \quad (13)$$

The statistical description of the system coupled to an unobserved bath is provided by the reduced density operator which is defined as

$$\hat{\rho}^I(t) = \mathrm{Tr}_B\{\hat{\sigma}^I(t)\}, \quad (14)$$

where Tr_B refers to the trace over all degrees of freedom of the bath. The equation of motion for the reduced density

operator is obtained, as usual,[34] by making use of the formal solution of the Liouville equation (10),

$$\hat{\sigma}^I(t) = \hat{\sigma}^I(0) + \frac{i}{\hbar}\int_0^t dt'\{[E_z(t')\mu_z^I(r,\phi,t') - \hat{H}_{SB}^I(r,\phi,\{q_i\},t'),\hat{\sigma}^I(t')]\}, \quad (15)$$

substituting Eq. (15) back into Eq. (10) and evaluating the trace (14) under the basic condition of irreversibility

$$\hat{\sigma}^I(t) = \hat{\rho}^I(t)\hat{\rho}_B(0), \quad (16)$$

where

$$\hat{\rho}_B(0) = \frac{e^{-\hat{H}_B/k_BT}}{\mathrm{Tr}_B\{e^{-\hat{H}_B/k_BT}\}}. \quad (17)$$

Finally, one obtains the equation of motion for the reduced density operator

$$\frac{\partial\hat{\rho}^I(t)}{\partial t} = \frac{i}{\hbar}E_z(t)[\mu^I(r,\phi,t),\hat{\rho}^I(t)] - \frac{1}{\hbar^2}\hat{R}^I(r,\phi,t), \quad (18)$$

where $\hat{R}^I(r,\phi,t)$, which will be referred to as the time-dependent relaxation operator, is given in the interaction picture by the following equation:

$$\begin{aligned}\hat{R}^I(r,\phi,t) &= \hat{R}_1^I(r,\phi,t) + \hat{R}_2^I(r,\phi,t)\\ &= \sum_i^{N_B}\int_0^t dt'\{[\lambda_i^I(r,\phi,t),\lambda_i^I(r,\phi,t')\hat{\rho}^I(t')]\\ &\times\langle Q_i(t)Q_i(t')\rangle - [\lambda_i^I(r,\phi,t),\hat{\rho}^I(t')\lambda_i^I(r,\phi,t')]\\ &\times\langle Q_i(t')Q_i(t)\rangle\}\\ &+ \frac{1}{2}\sum_i^{N_B}\sum_j^{N_B}\int_0^t dt'\{[\Lambda_{ij}^I(r,\phi,t),\Lambda_{ij}^I(r,\phi,t')\hat{\rho}^I(t')]\\ &\times\langle Q_{ij}(t)Q_{ij}(t')\rangle - [\Lambda_{ij}^I(r,\phi,t),\hat{\rho}^I(t')\Lambda_{ij}^I(r,\phi,t')]\\ &\times\langle Q_{ij}(t')Q_{ij}(t)\rangle\}. \end{aligned} \quad (19)$$

The overall relaxation operator $\hat{R}^I(r,\phi,t)$ consists of two parts, $\hat{R}_1^I(r,\phi,t)$ accounting for one-phonon relaxation and $\hat{R}_2^I(r,\phi,t)$ accounting for two-phonon relaxation. The time correlation functions $\langle Q_i(t)Q_i(t')\rangle$ and $\langle Q_{ij}(t)Q_{ij}(t')\rangle$ in Eq. (19) are defined by the following equations:

$$\langle Q_i(t)Q_i(t')\rangle = \mathrm{Tr}_B\{q_i^I(t)q_i^I(t')\hat{\rho}_B(0)\}, \quad (20)$$

where $\langle Q_i(t')Q_i(t)\rangle = \langle Q_i(t)Q_i(t')\rangle^*$ and

$$\langle Q_{ij}(t)Q_{ij}(t')\rangle = \mathrm{Tr}_B\{q_i^I(t)q_j^I(t)q_i^I(t')q_j^I(t')\hat{\rho}_B(0)\}, \quad (21)$$

where $\langle Q_{ij}(t')Q_{ij}(t)\rangle = \langle Q_{ij}(t)Q_{ij}(t')\rangle^*$. It is easy to show that

$$\langle Q_{ij}(t)Q_{ij}(t')\rangle = \langle Q_i(t)Q_i(t')\rangle\langle Q_j(t)Q_j(t')\rangle. \quad (22)$$

For the bath represented by normal modes (an ensemble of harmonic oscillators) [see Eq. (7)] it can be shown that the time correlation function for one-phonon transitions, $\langle Q_i(t)Q_i(t')\rangle$, has the following form:

$$\langle Q_i(t)Q_i(t')\rangle = \frac{\hbar}{2M_i\omega_i}\Phi(\omega_i,t-t',T),$$

$$\begin{aligned}\Phi(\omega_i,t-t',T) &= [\bar{n}(\omega_i)+1]\exp[-i\omega_i(t-t')]\\ &+ \bar{n}(\omega_i)\exp[i\omega_i(t-t')],\end{aligned} \quad (23)$$

where

$$\bar{n}(\omega_i) = \frac{1}{\exp(\hbar\omega_i/k_BT)-1} \quad (24)$$

is the Bose-Einstein distribution function. The time correlation functions for two-phonon transitions, $\langle Q_{ij}(t)Q_{ij}(t')\rangle$, are easily obtained from Eq. (22).

Equation of motion (18) has been treated numerically in the system-state representation. Taking matrix elements between the system eigenstates $|v\rangle = \psi_v(r,\phi)$, one gets

$$\frac{d\rho_{vv'}^I(t)}{dt} = \frac{i}{\hbar}E_z(t)[\mu_z^I(t),\hat{\rho}^I(t)]_{vv'} - \frac{1}{\hbar^2}[R_{1vv'}^I(t) + R_{2vv'}^I(t)]. \quad (25)$$

The matrix elements of operators in Eq. (25) in the interaction picture are related to the Schrödinger picture as follows:

$$B_{vv'}^I(t) = e^{i\omega_{vv'}t}\langle\psi_v(r,\phi)|B(r,\phi)|\psi_{v'}(r,\phi)\rangle, \quad (26)$$

where $B=\mu_z$, λ_i, and Λ_{ij}, respectively. The one-phonon relaxation matrix $R_{1vv'}^I(t)$ in Eq. (25) reads

$$\begin{aligned}R_{1vv'}^I(t) &= \sum_i^{N_B}\frac{\hbar}{2M_i\omega_i}\int_0^t dt'\{[\lambda_i^I(t),\lambda_i^I(t')\hat{\rho}^I(t')]_{vv'}\\ &\times\Phi(\omega_i,t-t',T) - [\lambda_i^I(t),\hat{\rho}^I(t')\lambda_i^I(t')]_{vv'}\\ &\times\Phi^*(\omega_i,t-t',T)\},\end{aligned} \quad (27)$$

where $\Phi(\omega_i,t-t',T)$ is given by Eq. (23). It has been treated explicitly by making use of the 3D arrays $\{i,v,v'\}$ with Eq. (26) (for $B=\lambda_i$) and results given in Appendix B of Ref. 2.

The explicit treatment of the two-phonon relaxation with matrix $R_{2vv'}^I(t)$ is too expensive, therefore a quasiresonant model, similar to those used in our previous works,[16,24] and a partial averaging over one of two bath variables have been involved as described below. The two-phonon relaxation matrix in the system-state representation reads

$$\begin{aligned}R_{2vv'}^I(t) &= \frac{\hbar^2}{8}\sum_i^{N_B}\sum_j^{N_B}\int_0^t dt'\left\{\frac{[\Lambda_{ij}^I(t),\Lambda_{ij}^I(t')\hat{\rho}^I(t')]_{vv'}}{M_i\omega_iM_j\omega_j}\right.\\ &\times\Phi(\omega_i,t-t',T)\Phi(\omega_j,t-t',T)\\ &- \frac{[\Lambda_{ij}^I(t),\hat{\rho}^I(t')\Lambda_{ij}^I(t')]_{vv'}}{M_i\omega_iM_j\omega_j}\\ &\left.\times\Phi^*(\omega_i,t-t',T)\Phi^*(\omega_j,t-t',T)\right\}.\end{aligned} \quad (28)$$

A partial averaging over the j coordinate of the bath yields

$$R^I_{2vv'}(t) \Rightarrow \frac{\hbar^2}{8}\sum_i^{N_B}\int_0^t dt'\left\{\frac{[\Lambda_i^I(t),\Lambda_i^I(t')\hat{\rho}]^I(t')]_{vv'}}{M_i\omega_i}\right.$$
$$\times\sum_j^{N_B}\Phi(\omega_i,t-t',T)\Phi(\omega_j,t-t',T) - \frac{[\Lambda_i^I(t),\hat{\rho}^I(t')\Lambda_i^I(t')]_{vv'}}{M_i\omega_i}$$
$$\left.\times\sum_j^{N_B}\Phi(\omega_i,t-t',T)^*\Phi(\omega_j,t-t',T)^*\right\}, \tag{29}$$

where the products of the matrix elements between the system states for the two-phonon transitions are defined as follows:

$$\Lambda_i^I(t)_{vk}\Lambda_i^I(t')_{nv'} = \frac{1}{N_B}\sum_j^{N_B}\frac{\Lambda_{ij}^I(t)_{vk}\Lambda_{ij}^I(t')_{nv'}}{M_j\omega_j}. \tag{30}$$

The products of the matrix elements given by Eq. (30) have been calculated in the Schrödinger picture by making use of the results given in Appendix B of Ref. 2, see Eq. (33) therein, and subsequently transformed into the interaction picture with Eq. (26) (for $B=\Lambda_{ij}$).

A quasiresonant model for the two-phonon relaxation has been employed as follows. Taking into account that the most efficient energy exchange among coupled systems occurs in the case of the resonance, it is reasonable to assume that the two-phonon relaxation depends on the bath frequency ω_j in a resonant way with respect to any system frequency $\omega_{mn}=(E_m-E_n)/\hbar$ and the other bath frequency ω_i. Specifically, similar to our previous works,[16,24] the following substitution is made in Eq. (29):

$$\sum_j^{N_B}\Phi(\omega_i,t-t',T)\Phi(\omega_j,t-t',T)\Rightarrow\sum_{m=1}^{v_{\max}}\sum_{n=0}^{m-1}\int_{A_{mn}}^{B_{mn}}\Phi(\omega_i,t-t',T)\Phi(\Omega,t-t',T)g_{mni}(\Omega)d\Omega, \tag{31}$$

where $A_{mn}<\omega_{mn}<B_{mn}$ and $g_{mni}(\Omega)$ is represented by a Lorentzian-type distribution function

$$g_{mni}(\Omega) = \frac{1}{\pi}\frac{\gamma_{mn}}{\gamma_{mn}^2+[(\omega_{mn}-\omega_i)-\Omega]^2}, \tag{32}$$

which has a maximum at $\Omega=\omega_{mn}-\omega_i$, and $\gamma_{mn}>0$ determines the width of the distribution (32), corresponding to a combined system-bath frequency $\omega_{mn}-\omega_i$. The γ_{mn} are treated here as empirical parameters, determined from criteria to be discussed below. Within the quasiresonant model used here, we keep only the sum frequencies $\omega_i+\omega_j$ in Eq. (31) and suppose that the Bose-Einstein distribution functions $\bar{n}(\Omega)$ can be reasonably approximated by their "central values" $\bar{n}(\omega_{mn}-\omega_i)$ in each frequency interval $A_{mn}\leqslant\Omega\leqslant B_{mn}$. Taking into account that the bath is supposed to be in thermal equilibrium at all times, we assume that the energy exchange among the system and the bath at a certain system frequency ω_{mn} is not affected by those occurring at other system frequencies. We therefore allow the respective distributions $g_{mni}(\Omega)$ defined by Eq. (32) to be overlapping and set $A_{mn}=-\infty$ and $B_{mn}=\infty$. This yields tabulated integrals[35] in Eq. (31), which finally reads as follows:

$$\sum_j^{N_B}\Phi(\omega_i,t-t',T)\Phi(\omega_j,t-t',T)\Rightarrow\sum_{m=1}^{v_{\max}}\sum_{n=0}^{m-1}\exp(-\gamma_{mn}|t-t'|)\{[\bar{n}(\omega_i)+1][\bar{n}(\omega_{mn}-\omega_i)+1]\exp[-i\omega_{mn}(t-t')]\bar{n}(\omega_i)$$
$$\times\bar{n}(\omega_{mn}-\omega_i)\exp[i\omega_{mn}(t-t')]\}. \tag{33}$$

It is clearly seen from Eqs. (29) and (33) that, with the quasiresonant model for the two-phonon relaxation being employed together with the partial averaging over one of two bath variables, the two-phonon relaxation matrix $R^I_{2vv'}(t)$ (28) can be treated in the equation of motion (25) by making use of the 3D arrays $\{i,v,v'\}$ [i.e., similar to the one-phonon relaxation matrix $R^I_{1vv'}(t)$, see Eq. (27)].

Equation (25) is the basic equation of motion in the present work for the investigation of the non-Markovian dissipative quantum dynamics of the system driven by the IR laser field. Through the relaxation terms, it depends on all previous times. It has been solved by using several modifications of standard numerical methods,[36] in particular, the Adams-Bashforth-Moulton schemes for a predictor-corrector method similar to our previous works.[16,24,37–39] The initial conditions to Eq. (25),

$$\rho^I_{vv'}(t=0) = \frac{e^{-E_v/k_BT}}{\sum_{v''}e^{-E_{v''}/k_BT}}\delta_{v'v}, \tag{34}$$

correspond to the thermal equilibrium of the system and the bath at temperature T (typically, $T=4$ K). The solution of Eq. (25) yields the reduced density matrix elements $\rho^I_{vv'}(t)$ and, in particular, the time-dependent populations

$$P_v(t) = \rho^I_{vv}(t). \tag{35}$$

B. Markovian theory

From the above theory, a Markovian approximation could be derived along the lines of Ref. 34, for example. Instead, we use a slightly more pragmatic approach, namely the Mar-

kovian theory based on Lindblad operators, similar to Refs. 2 and 40. Accordingly, the equations of motion in the Schrödinger picture and explicitly written out in the basis of N system eigenstates are

$$\frac{d\rho_{vv}}{dt} = \frac{i}{\hbar}E_z(t)\sum_{v'=0}^{N-1}(\mu_{vv'}\rho_{v'v} - \rho_{vv'}\mu_{v'v}) + \sum_{v'=0}^{N-1}(\Gamma_{v'\to v}\rho_{v'v'} - \Gamma_{v\to v'}\rho_{vv}) \tag{36}$$

for the diagonal elements of the reduced density matrix and

$$\frac{d\rho_{v'v}}{dt} = -i\omega_{v'v}\rho_{v'v} + \frac{i}{\hbar}E_z(t)\sum_{v''=0}^{N-1}(\mu_{v'v''}\rho_{v''v} - \rho_{v'v''}\mu_{v''v}) - \gamma_{v'v}\rho_{v'v} \tag{37}$$

for the off-diagonal elements. In Eq. (36), $\mu_{v'v}$ are the transition dipole moments defined in Eq. (6), and the $\Gamma_{v'\to v}$ are the relaxation rates, which were calculated from a Golden Rule treatment in Ref. 2, see also Table I. In Eq. (37), $\gamma_{v'v}$ is a dephasing rate, given as $\gamma_{v'v}=\gamma_{vv'}=\frac{\Gamma_{v'\to v}}{2}$ if pure dephasing[41] is neglected. This assumption is reasonable in our case, as also discussed in Ref. 40, where it was shown that pure dephasing is expected to be of minor importance for IR excitation. Nevertheless, treatment of pure dephasing should be included in the future work. Since the transition rates do not depend on previous times, Eqs. (36) and (37) contain no memory, and were solved with a Newton polynomial propagator.[42]

C. Choice of electric field $E_z(t)$

Two strategies were used to determine suitable electric fields $E_z(t)$. In a first strategy, which is used in particular in conjunction with the non-Markovian theory, we employ one or two laser pulses of $\sin^2$ form,

$$E_z(t) = E_{0,1}\sin^2\left[\frac{\pi(t-t_{s_1})}{t_{p_1}}\right]\sin(\omega_{l_1}t+\varphi_1) + E_{0,2}\sin^2\left[\frac{\pi(t-t_{s_2})}{t_{p_2}}\right]\sin(\omega_{l_2}t+\varphi_2), \tag{38}$$

where $E_{0,k}$, $k=1,2$, is the amplitude of the kth pulse, t_{s_k} its starting time, t_{p_k} its duration, ω_{l_k} the respective laser carrier frequency, and φ_k the phase. These parameters are optimized iteratively "by hand" to achieve a specific goal.[43]

A more systematic strategy is optimal control theory (OCT) for open quantum systems, as in Ref. 28 This approach was exclusively used here for the Markovian case. Accordingly, we maximize the constrained functional

$$J = \langle\langle\hat{O}|\hat{\rho}(t_p)\rangle\rangle - \int_0^{t_p}\alpha(t)|E_z(t)|^2dt - \int_0^{t_p}dt\left\langle\langle\hat{\sigma}(t)|\frac{\partial}{\partial t} + \frac{i}{\hbar}[\mathcal{L}_H+\mathcal{L}_D]|\hat{\rho}(t)\rangle\right\rangle. \tag{39}$$

$\hat{O}$ is a target operator (e.g., the projection operator on a vibrational eigenstate) whose expectation value, expressed here in double space notation, $\langle\langle\hat{O}|\hat{\rho}(t_p)\rangle\rangle := \mathrm{Tr}\{\hat{O}^\dagger\hat{\rho}(t_p)\}$ is to be maximized at time t_p, the end of the pulse. $\alpha(t)$ is a time-dependent penalty factor to keep the pulse fluence (second term) low. As another constraint the open-system Liouville-von Neumann equation has to be fulfilled (third term), with $\mathcal{L}_H$ and $\mathcal{L}_D$ denoting the Hamiltonian and dissipative Liouvillians, respectively (see Ref. 40 for details). $\hat{\sigma}(t)$ is a Lagrange density operator to enforce this second constraint. The variational calculus leads to coupled equations for the field, the density operator $\hat{\rho}$, and the Lagrange multiplier $\hat{\sigma}$, which can be solved with an iterative scheme, see Refs. 28 and 40. The electric field is then computed from

$$E_z(t) = -\frac{1}{\hbar\alpha}\mathrm{Im}\langle\langle\hat{\sigma}(t)|\hat{\mu}_z|\hat{\rho}(t)\rangle\rangle. \tag{40}$$

Further, a rounded plateau function

$$\alpha(t) = \begin{cases} \alpha_0\sin^2\left(\dfrac{4\pi t}{t_p}\right) & \text{for } 0 \le t \le t_p/8, \\ \alpha_0\sin^2\left(\dfrac{4\pi t}{7t_p}\right) & \text{for } 7t_p/8 \le t \le t_p, \\ \alpha_0 & \text{else} \end{cases} \tag{41}$$

was chosen to produce optimal pulses which go smoothly to zero toward the beginning and the end of the pulse.

To analyze the pulses, we either simply consider their time evolution $E_z(t)$ or compute the Husimi quasiprobability distribution $P_H(t,E)$ in time-energy space.[44] The Husimi distribution is obtained from smoothing a Wigner distribution $P_W(t,E)$ with a Gaussian in time and energy, as outlined in Ref. 40.

IV. RESULTS AND DISCUSSION

A. Free evolution of excited vibrational states

First the widths γ_{mn} of the Lorentzian distribution function (32) have been chosen such as to reproduce the lifetimes of the system states calculated previously in Ref. 2. The variation of γ_{mn} in the interval of 6–8 cm^{-1} made it possible to achieve a good agreement with the results of Ref. 2. Two examples are presented in Figs. 1(a) and 1(b). It is assumed that the system is prepared initially in a certain system state $v(v_r,v_\phi)$ [$v=5$, corresponding to (0,4) in Fig. 1(a) and $v=8$, corresponding to (1,2) in Fig. 1(b), respectively], and then the non-Markovian equation of motion (25) is propagated at the laser field $E_z(t)=0$. For comparison, also the population dynamics arising from the Markovian model (36) and (37) is shown.

Comparison of the non-Markovian free relaxation to the Markovian one shows first of all that the population decay of the initial state proceeds indeed (by construction) on very similar timescales. A first difference between the two models is that the non-Markovian population dynamics of the initial state is nonexponential (Gaussian-like), with $\lim_{t\to 0} dP/dt = 0$, in contrast to the Markovian theory which is exponential. If, as in the examples shown, the decay proceeds along a

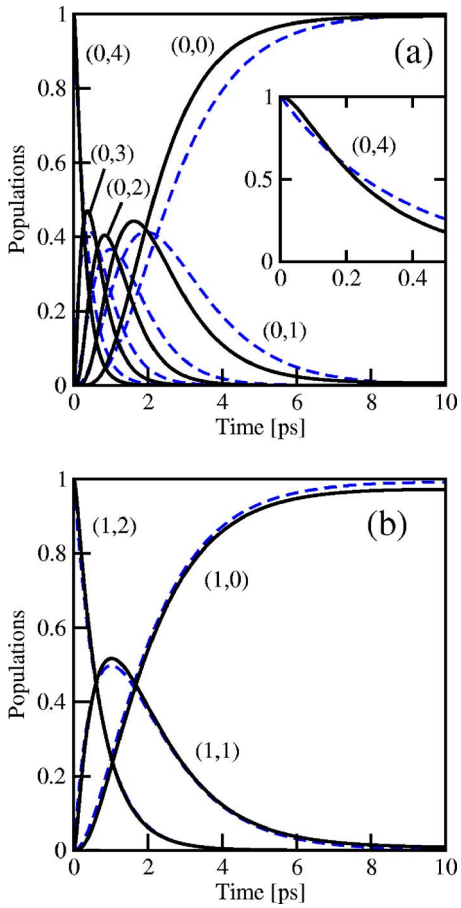

FIG. 1. (Color online) Free evolution of eigenstates (a) $v=5$ (0,4) and (b) $v=8$ (1,2) at $T=4$ K, for the non-Markovian (solid) and Markovian models (dashed), during the first 10 ps. The inset in (a) shows dynamics of (0,4) within the first 0.5 ps.

"vibrational ladder," it is also observed that for Markov and non-Markov the maxima of populations of individual levels occur at different times, and possibly with different amplitudes.

B. Mode-selective excitation of adsorbate vibrations with shaped infrared laser pulses

From Table I and Ref. 2 we know that the characteristic features of the H/Si model considered here are (i) very different frequencies for the r and ϕ modes, (ii) weak r-ϕ coupling within the subsystem, (iii) small anharmonicity of both modes, (iv) very different timescales for the relaxation of the r (ns timescale) and ϕ modes (picosecond timescale), and, finally, (v) transition dipole moments for r excitation which are an order of magnitude larger than for ϕ excitation. As a consequence of (i) and (ii) we expect that mode-selective excitation by tailored IR pulses should be possible. Items (iv) and (v) lead to the expectation that this excitation may be more difficult to achieve and preserve for the ϕ mode. Finally, from item (iii) one can expect that state-selectivity is harder to achieve than mode-selectivity.

1. Mode- and state-selective excitation of the Si-H stretching mode

The long-lived stretching levels $(v_r,0)$ can indeed be selectively prepared with the probability close to 100% by optimally tailored IR laser pulses. The example presented in Fig. 2(a) shows the population dynamics in the case of selective preparation of state (1,0) by a single, optimal laser pulse of $\sin^2$ shape [see Eq. (38)]. It is seen from Fig. 2 that a 1-ps laser pulse can provide almost complete population transfer to the target level.

The pulse has been optimized by iteratively adjusting the parameters E_0 and ω_l, and fixing $\varphi=0$. For the optimization, the non-Markovian theory was chosen with the lowest 50 states considered, and $T=4$ K. The optimal frequency $\omega_l \approx 2041.7$ cm^{-1} is almost equal to the resonance frequency of $\omega_r \approx 2042$ cm^{-1}, and the field amplitude $E_0 = 3.8652$ MV/cm is very close to $E_0^{\pi} = \frac{2\pi\hbar}{t_p|\mu_{04}|} = 3.7977$ MV/cm. This latter quantity is the field amplitude of a π pulse, estimated from a two-level system in the rotating wave approximation, when in addition relaxation is neglected and $T=0$ K.[40]

With a shorter (0.5 ps) laser pulse [Fig. 2(b)], the optimal field amplitude increases $\propto t_p^{-1}$, and the final population of the target state (1,0) is slightly lower (in the order of 95%), due to the population of other, nonresonant, stretching states (2,0) and (3,0). The activation of nonresonant transitions in a strong IR laser field implies that the stretching levels $(v_r,0)$ can be excited, perhaps up to the desorption continuum, by quasiresonantly pumping the r mode. This possibility will be addressed in a separate work.[45] If (sub-) ps laser pulses are used for vibrational excitation of the r mode, pumping is also not perturbed by energy relaxation, because the latter proceeds on a timescale about three times longer than the excitation process. In summary, mode- and even state-selective excitation of the Si-H stretch mode should be possible with ps-IR pulses.

The same laser fields (a) and (b) as in Fig. 2 have also been used in the Markovian model according to Eqs. (36) and (37), again with 50 vibrational states and $T=4$ K. In the lowest panels of Fig. 2 the differences in populations, $P_v^{\text{non-Markov}} - P_v^{\text{Markov}}$ are shown, and found to be small. In particular, the final populations are almost unaffected—differences are then only due to the fact that the field is no longer optimal. The good agreement between Markov and non-Markov shows that energy relaxation plays a minor role on the timescale considered, and hence any additional approximations to treat it lead to marginal differences only.

2. Mode-selective excitation of the Si-H bending mode

While the IR excitation of the Si-H stretch mode appears to be straightforward, the bending mode is not so easy to excite with ps pulses. This is due to the short (ps) vibrational lifetimes of the $(0,v_\phi)$ states on the one hand, and unfavourable transition dipole moments on the other (see Table I). In addition, the bending mode is, in our model at least, more harmonic than the stretch mode (see Table 3 of Ref. 2), thus a *state-selective* control will be difficult

Low-energy excitations. In Fig. 3 various situations and/or

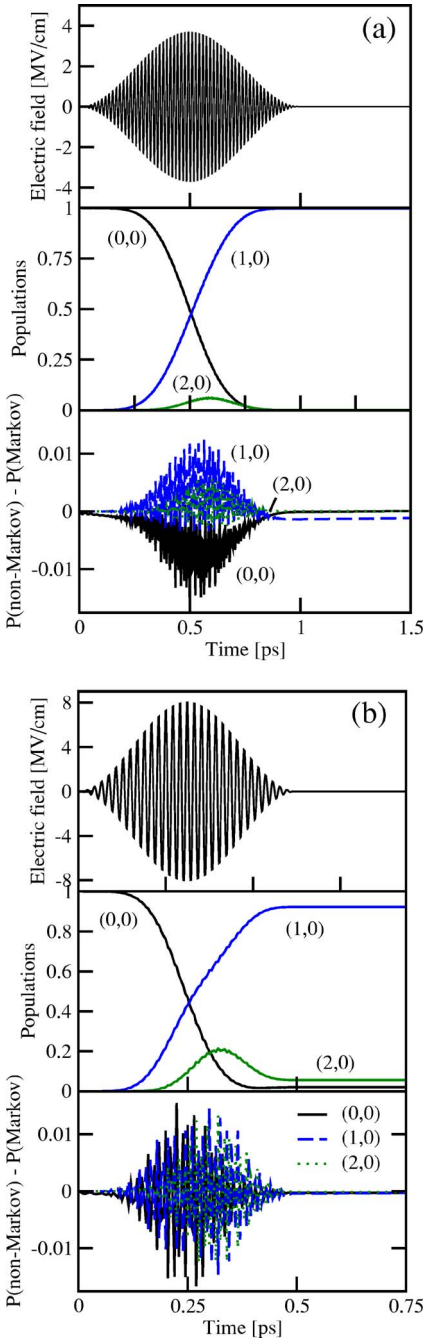

FIG. 2. (Color online) Selective preparation of the stretching state (1,0) by optimal $\sin^2$ pulses with $t_p=1$ ps (a) and $t_p=0.5$ ps (b), for $T=4$ K. The laser pulse parameters are $E_1^{(a)}=3.8652$ MV/cm, $\omega_l^{(a)}=2041.709$ cm−1, $E_1^{(b)}=8.41696$ MV/cm and $\omega_l^{(b)}=2060.563$ cm−1. In both cases the electric field (top panel), population dynamics (middle panel, Markov and non-Markov results are almost indistinguishable on this scale), and the population differences between non-Markov and Markov are shown (lowest panel).

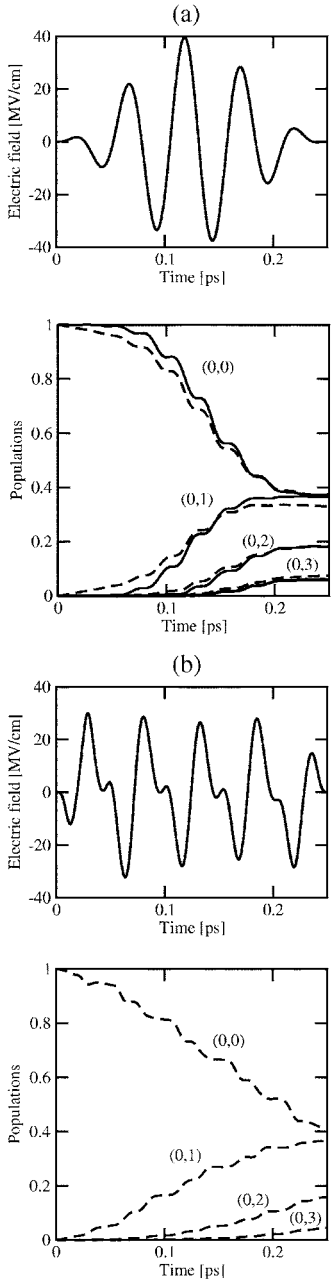

FIG. 3. Optimal pulses to excite the bending state $v=1$ (0,1) vibrational state at $T=4$ K with pulses of length $t_p=0.25$ ps. Displayed in (a), upper panel is the electric field of a $\sin^2$ pulse, optimized within the non-Markovian model with 50 states ($E_0=39.8761$ MV/cm, $\omega_l=635.1757$ cm−1). Displayed in (b), upper panel is the electric field of an optimal control pulse, obtained within the Markov model with 22 states. The lower panels show selected time-resolved populations, when the pulses above have been used either within the non-Markovian theory (solid line) or the Markov theory (dashed lines), respectively.

models are considered, in which laser pulses were designed to selectively excite the Si-Si-H bending mode. Short pulses were used to beat dissipation. In Fig. 3(a) we show a single $\sin^2$ pulse, with a pulse duration t_p of only 0.25 ps for which the field amplitude and frequency were optimized at fixed $t_{s_1}=0$ and $\phi_1=0$ with the goal to populate $v=1$ (0,1). For that purpose, the non-Markovian theory has been used, and 50 vibrational states were considered at $T=4$ K as before. Corresponding selected level populations are shown as solid lines in the lower panel of Fig. 3(a).

The maximal population of the target state at the end of the pulse achieved during optimization is 0.3646. Similar results are obtained with optimized 0.5 ps, and 88.8 fs laser pulses, i.e., neither longer nor shorter pulses improve state-selectivity considerably. The total excitation probability $1-P_0(t_p)$ is about 0.64, showing that the initial state cannot be entirely depopulated when the dissipation is strong.[40] On the other hand, the excitation is highly *mode selective*: After the pulse is off, the populated excited states are almost exclusively $(0,v_\phi)$, with $v_\phi=1,2,3,\ldots$. The notion of mode selectivity will be quantified below. The population of the $(0,v_\phi)$ excited levels is the largest for $v_\phi=1$ and rapidly decreases with increasing v_ϕ. For $v_\phi=1-3$ they are all significant, however. This is a consequence of the harmonicity of the ϕ mode in our model. Hence the laser frequency is resonant also for higher states which can then easily be excited.

It is no surprise, then, that the optimal laser frequency is almost resonant with the ϕ mode ($\omega_\phi=637$ cm^{-1}). The optimized field amplitude of 39.8761 MV/cm is clearly smaller than the ideal π pulse value of $E_0^\pi=\frac{2\pi\hbar}{t_p|\mu_{01}|}=61.8368$ MV/cm, showing that in this case the idealization as a dissipation-free two-level system does not hold. The optimized field amplitude is by more than a factor of 10 larger than that for *r*-mode excitation, due to the smaller transition dipole moment.

For comparison, the dynamics in Markovian approximation obtained with that same pulse is also shown in Fig. 3(a), lower panel, as dashed lines. One can see that the difference between non-Markovian and Markovian time evolution affects mostly the initial dynamics where the population gradients at $t=0$ are zero in the non-Markovian case, and change less rapidly initially. After the pulse is off, the target state population is slightly less with Markov than with non-Markov. Altogether, non-Markovian behavior appears to be small, however.

The question arises as to whether optimal control pulses would lead to an even higher excited state population and/or to state selectivity. To address this question, an OCT pulse was generated within the Markovian theory, realized within a vibrational state basis consisting of the 22 lowest eigenstates (which proved to be sufficient), and by choosing as target operator the projector on the $v=1$ (0,1) eigenstate, $\hat{O}=|1\rangle\langle 1|$. It can be seen from Fig. 3(b), upper panel, that the resultant pulse is more structured than the sin^2 pulse. Closer inspection based on the Husimi distribution of the pulse shows that it contains a main frequency around ω_ϕ, but also a second, weaker feature with a frequency about $2\omega_\phi$. This indicates a certain amount of overtone excitation. This detail obviously enhances the final population of the target state (0,1) slightly, relative to Fig. 3(a) (with Markov approximation), despite the peak intensity of the OCT pulse ebbing smaller than that of the sin^2 pulse. The final population of state (0,1), obtained with pulses (a) and (b), respectively, is 0.3301 for (a) and 0.3636 for (b), respectively, when fed in the Markovian equations of motion (dashed curves in Fig. 3). Thus there is slightly enhanced state selectivity under optimal control conditions. The total excitation probability $P_{\rm ex}(t_p)=1-P_0(t_p)$ on the other hand, is somewhat lower than with the sin^2 pulse, namely 0.6262 [for (a)], and 0.5781 [for (b)]. This quantity, however, was also not optimized in the OCT calculations. The mode selectivity is and remains high in both cases. Defining the ϕ-mode selectivity as

$$S_\phi=\frac{P_\phi}{P_{\rm ex}}, \tag{42}$$

where P_ϕ is the sum of populations in exclusively ϕ-excited states $(0,v_\phi)$, $v_\phi=1,2,3,\ldots$, one finds $S_\phi=0.993$ for field (a) and $S_\phi=0.991$ for field (b). A further improvement is expected from using optimal control pulses which are obtained by solving non-Markovian equations of motion, which was not attempted here.

In summary, mode-selective excitation is possible also for the ϕ mode. On the other hand, state selectivity is harder to achieve. It must also be noted that after the pulse is off the ϕ-excited states will rapidly relax.

High-energy excitations. As mentioned above, using a single, short pulse optimized for the $(0,0)\rightarrow(0,1)$ transition populates also higher ϕ states, however, with a probability that decreases rapidly with increasing v_ϕ. For example, by using the sin^2 pulse (a) in Fig. 3 and the Markovian equations of motion, the population of the (0,11) state is only 1.3×10^{-6} after the pulse is off. To excite higher vibrational levels $(0,v_\phi)$ with siginificant probability, the pulses must be reoptimized. These high-energy excitations may be useful, for example, if one is interested to enforce lateral motion of H on the surface, i.e., diffusion. Since the higher-excited states are more strongly coupled to the substrate phonons, this not only leads to shorter vibrational lifetimes [see Table I and Ref. 2, according to which approximately $\tau(v_\phi)\propto 1/v_\phi$], and consequently also to larger differences between Markovian and non-Markovian models. Further, the higher-excited states show stronger intermode couplings by the potential and the transition dipole moments.

In Fig. 4 we use a sin^2 pulse which was obtained with the goal to maximize the population in the $v=26$ (0,11) vibrational state. Typically, longer laser pulses should be used to prepare higher states, because shorter pulses require stronger fields which decrease state selectivity. In Fig. 4(a), we show selected populations which were obtained with a single sin^2 pulse 1 ps long whose field amplitude and frequency were optimized within the non-Markovian model, with 50 states in total and $T=4$ K.

It is found in this model, that the high-lying target state is populated with high probability, $P_{26}(t_p)=0.3576$ after the pulse is off. From the P_ϕ curve which gives the population in all exclusively ϕ-excited states, it is also noted that the excitation is highly bond selective. In fact, the entire ϕ-vibrational ladder is populated, however, with a clear maximum around $v_\phi=11$. For example, the two levels $v=22$ (0,10) and $v=30$ (0,12), i.e., the nearest neighbors of the target state along the vibrational ladder carry the largest populations apart from the target state, but their population is already clearly smaller: $P(0,10)(t_p)=0.1315$, $P(0,12)(t_p)=0.1464$. The initial state is almost empty at the end of the pulse, hence $P_\phi(t_p)$ is equal to the bond selectivity defined in Eq. (42). The optimal laser frequency is still close to the

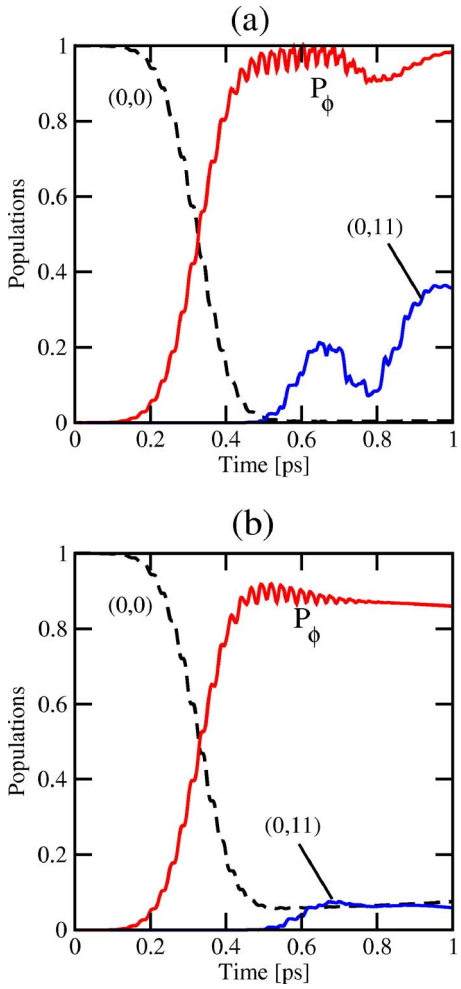

FIG. 4. (Color online) Excitation of high-energy bending states, by optimizing the population of the $v=26$ (0,11) level with a single laser pulse at $T=4$ K, using the non-Markovian model. (a) Selected populations for the non-Markovian calculation. (b) Selected populations if the same pulse is used within the Markovian model. The $\sin^2$ laser pulse parameters for both cases are $t_p=1.0$ ps, $E_0=44.7711$ MV/cm, $\omega_l=642.3097$ cm^{-1}.

frequency of the bending mode ($\omega_l \approx 642$ cm^{-1}), while the maximal field amplitude is slightly higher than in the "low-energy" case considered in Fig. 3 ($E_0 \approx 45$ MV/cm). Since the chosen pulse is now also longer, the laser fluence is higher (by a factor of 5.04) than that of the pulse in Fig. 3(a).

When using the optimized $\sin^2$ pulse for the Markovian equations of motion, the resulting populations are now distinctly different from the non-Markovian ones [Fig. 4(b)]. The final target-state population is only $P(0,11)(t_p)=0.0589$. Also, bond selectivity is lost to some extent. Still, the excitation of the ϕ mode clearly dominates, but now the final $P(0,v_\phi)$ populations reflect a broader distribution. Even the ground vibrational state is not empty, and up to $v_\phi \approx 13$ the population is significant. In fact, $v_\phi=11$ is not the maximum of the distribution: $P(0,10)(t_p)=0.0693$, $P(0,12)(t_p)=0.0413$ at the end of the pulse.

Thus, in contrast to the low-energy excitation of Fig. 3, large differences between Markovian and non-Markovian theories are observed. This might have been expected in view of the mentioned fact that dissipation is stronger for higher-excited states, and hence any additional approximations to treat it will matter. In summary, one can say that the Markov approximation overestimates both energy relaxation and intermode coupling if high-energy states with large decay rates and also large transition dipole moments to nearby states are considered.

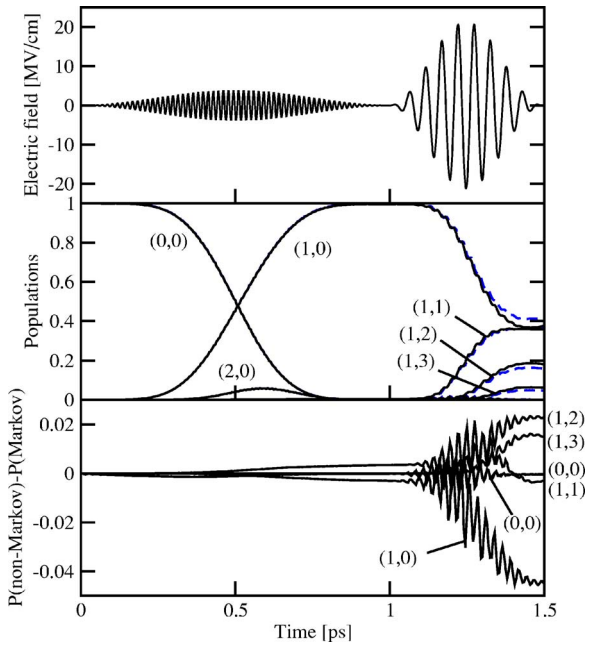

FIG. 5. (Color online) Preparation of $(1,v_\phi)$ states, by two non-overlapping $\sin^2$ laser pulses of the form (38). Optimization was done within the non-Markov model, with 50 states and $T=4$ K. The laser pulse parameters are $t_{p_1}=1$ ps, $E_{0,1}=3.8652$ MV/cm, $\omega_{l_1}=2041.709$ cm^{-1} ($t_{s_1}=0$ and $\varphi_1=0$ fixed); $t_{p_2}=0.5$ ps, $E_{0,2}=21.1916$ MV/cm, $\omega_{l_2}=636.3223$ cm-1 ($t_{s_2}=1$ ps and $\varphi_2=0$ fixed). The electric field (top panel), population dynamics (middle panel; non-Markov: solid; Markov: dashed), and the population differences between non-Markov and Markov (lowest panel) are depicted.

To achieve higher target-state populations also in the Markovian case, in analogy to Fig. 3(b) optimal control theory was used in conjunction with the Markovian equations of motion. In fact it is then found (but not shown here), that OCT pulses can be created which indeed increase the target-state population considerably in comparison to the $\sin^2$/Markov model. However, a population as large as with the sin $\sin^2$/non-Markov model was (so far) not obtained. One point learned from these preliminary OCT calculations is again that the optimal pulses exhibit a more complex time-frequency pattern.

3. Selective preparation of $(v_r=1,v_\phi)$ states

The $(v_r>0,v_\phi>0)$ states, which have vibrational energy in both stretching and bending degrees of freedom, can be prepared by the sequential excitation of the stretching and the bending vibrations, respectively.

An example is given in Fig. 5, where a field consisting of two $\sin^2$ pulses according to Eq. (38) is used. The non-

Markovian theory was used, with 50 states and $T=4$ K. The first pulse is the 1 ps pulse which was generated in Fig. 2(a) to enforce a selective $(0,0)\rightarrow(1,0)$ transition, i.e., state-selective excitation of the r mode. The second, 0.5 ps laser pulse was optimized to maximize the population in state $v=6$ (1,1), starting out of level (1,0). Again, the excitation of the bending mode is only bond selective, not state selective, i.e., also other states $(v_r=1, v_\phi>1)$ are populated with significant probability. Like in Fig. 3, however, the population of states with $v_\phi>0$ decreases rapidly with increasing v_ϕ.

When the same pulses are employed within the Markovian scheme, the population dynamics remains very similar. As can be seen from the lowest panel of Fig. 5, during the first pulse, when r is excited, the difference is negligible. During the second pulse which excites the ϕ mode, the deviation becomes somewhat larger. Again, this is a consequence of the fact that the r mode couples less efficient to the substrate phonons than the ϕ mode.

V. SUMMARY, CONCLUSIONS, OUTLOOK

In summary, bond-selective excitation of either the Si-H stretching or the Si-Si-H bending mode in H:Si(100)-2×1 has been studied, and is predicted, at least with the laser pulses used here, to be possible. The mode-selective excitation is possible because of the large mismatch between the frequencies of the r and ϕ modes, and an intermode potential coupling that is slow on the timescales considered here. (Intermode coupling occurs on a ns timescale within the present model, see Ref. 2.) On the timescale of picoseconds the high-frequency Si-H bond is also only weakly perturbed by vibration-phonon coupling, and state-selective excitations should be possible and stable for long times (~ns). In contrast, the lower-frequency Si-Si-H bending mode decays on a ps timescale. Within the system potential used here, only bond-selective excitation is possible for that mode which will in addition decay on the timescale of ps after preparation. On the other hand, for both stretching and bending modes the excitation of high-energy levels should be possible, with possible implications for IR-driven *reactions*, i.e., desorption and diffusion.

The Markov approximation holds well, if the excited vibrational states are only weakly coupled to the substrate phonons. This is particularly true for the lowest r-excited states, while ϕ excitation, in particular to higher states, is more sensitive to non-Markov effects. Both $\sin^2$ pulses and pulses obtained from optimal control theory were considered, the latter yielding sometimes slightly milder conditions.

Despite the fact that the present model can still be improved in many ways, we believe that it is already of relevance for IR excitation of real, hydrogen-covered Si surfaces. It may thus help to explain the recent observation of mode selectivity in IR laser induced desorption of H_2 from Si(111) surfaces.[20,21] The main difference to the laser excitation mechanism suggested here is that the experiment utilized a very narrow, fixed frequency laser tuned to the $v_r=0$ to $v_r=1$ transition in the H-Si stretching mode, effectively precluding any multiphoton excitation, since the anharmonicity in the H-Si stretching potential is already sufficient for the overtone excitations to be outside the laser line. However, we believe, that the present methodology can be adapted for that system, should laser parameters consistent with Ref. 20 be used. One can then hope to understand the experimental details and hence the still elusive reaction mechanism, in particular the unexpected (quadratic) scaling of the desorption yield with laser fluence.[20,21] Work along these lines is in progress in our laboratory.

ACKNOWLEDGMENTS

The authors acknowledge fruitful discussions with Y. Ohtsuki, Sendai, on optimal control theory. This work was financially supported by the Deutsche Forschungsgemeinschaft via the project Sa547/7, and also by SFB 450. G.K.P. acknowledges the hospitality and computer resources of the group of Manz at Freie Universität Berlin, during his stay there.

*Electronic address: petsaal@rz.uni-potsdam.de

[1] P. Guyot-Sionnest, P. H. Lin, and E. M. Miller, J. Chem. Phys. **102**, 4269 (1995).
[2] I. Andrianov and P. Saalfrank, J. Chem. Phys. **124**, 034710 (2006).
[3] Y.-C. Sun, H. Gai, and G. A. Voth, J. Chem. Phys. **100**, 3247 (1994).
[4] H.-F. Lu, M.-S. Ho, S.-C. Hong, A.-H. Liu, P.-F. Wu, and Y.-C. Sun, J. Chem. Phys. **109**, 6898 (1998).
[5] T.-C. Shen, C. Wang, G. C. Abeln, J. R. Tucker, J. W. Lyding, Ph. Avouris, and R. E. Walkup, Science **268**, 1590 (1995).
[6] E. T. Foley, A. F. Kam, J. W. Lyding, and Ph. Avouris, Phys. Rev. Lett. **80**, 1336 (1998).
[7] T. Vondrak and X.-Y. Zhu, Phys. Rev. Lett. **82**, 1967 (1999).
[8] C. Thirstrup, M. Sakurai, T. Nakayama, and K. Stokbro, Surf. Sci. **424**, L329 (1999).
[9] K. Stokbro, U. J. Quaade, R. Lin, C. Thirstrup, and F. Grey, Faraday Discuss. **117**, 231 (2000).
[10] A. Abe, K. Yamashita, and P. Saalfrank, Phys. Rev. B **67**, 235411 (2003).
[11] B. N. J. Persson and Ph. Avouris, Surf. Sci. **390**, 45 (1997).
[12] J. A. Prybyla, T. F. Heinz, J. A. Misewich, M. M. T. Loy, and J. H. Glownia, Phys. Rev. Lett. **64**, 1537 (1990).
[13] C. Springer, M. Head-Gordon, and J. C. Tully, Surf. Sci. **320**, (1994).
[14] F. F. Crim, Science **249**, 1387 (1990).
[15] P. Saalfrank and G. K. Paramonov, J. Chem. Phys. **107**, 10723 (1997).
[16] P. Saalfrank and G. K. Paramonov, J. Chem. Phys. **110**, 6500 (1999).
[17] P. Saalfrank and G. K. Paramonov, Chem. Phys. Lett. **301**, 509 (1999).

[18] K. Nakagami, Y. Ohtsuki, and Y. Fujimura, Chem. Phys. Lett. **360**, 91 (2002).
[19] I. Hussla, H. Seki, T. J. Chuang, Z. W. Gortel, H. J. Kreuzer, and P. Piercy, Phys. Rev. B **32**, 3489 (1985).
[20] Z. Liu, L. C. Feldman, N. H. Tolk, Z. Zhang, and P. I. Cohen, Science **312**, 1024 (2006).
[21] J. C. Tully, Science **312**, 1004 (2006).
[22] I. Andrianov and Saalfrank, Chem. Phys. Lett. **350**, 191 (2001).
[23] I. Andrianov and P. Saalfrank, Chem. Phys. Lett. **433**, 91 (2007).
[24] M. V. Korolkov and G. K. Paramonov, Phys. Rev. A **55**, 589 (1997).
[25] N. Wang, H. Rabitz, A. Manka, and C. Bowden, Phys. Rev. A **53**, R2940 (1996).
[26] A. Bartana, R. Kosloff, and D. J. Tannor, J. Chem. Phys. **106**, 1435 (1997).
[27] J. Cao, M. Messina, and K. Wilson, J. Chem. Phys. **108**, 1953 (1997).
[28] Y. Ohtsuki, W. Zhu, and H. Rabitz, J. Chem. Phys. **110**, 9825 (1999).
[29] D. T. Colbert and W. H. Miller, J. Chem. Phys. **96**, 1982 (1992).
[30] A. D. Becke, J. Chem. Phys. **98**, 5648 (1993).
[31] M. J. Frisch, G. W. Trucks, H. B. Schlegel, G. E. Scuseria, M. A. Robb, J. R. Cheeseman, V. G. Zakrzewski, J. A. Montgomery, Jr., R. E. Stratmann, J. C. Burant, S. Dapprich, J. M. Millam, A. D. Daniels, K. N. Kudin, M. C. Strain, O. Farkas, J. Tomasi, V. Barone, M. Cossi, R. Cammi, B. Mennucci, C. Pomelli, C. Adamo, S. Clifford, J. Ochterski, G. A. Petersson, P. Y. Ayala, Q. Cui, K. Morokuma, D. K. Malick, A. D. Rabuck, K. Raghavachari, J. B. Foresman, J. Cioslowski, J. V. Ortiz, A. G. Baboul, B. B. Stefanov, G. Liu, A. Liashenko, P. Piskorz, I. Komaromi, R. Gomperts, R. L. Martin, D. J. Fox, T. Keith, M. A. Al-Laham, C. Y. Peng, A. Nanayakkara, C. Gonzalez, M. Challacombe, P. M. W. Gill, B. Johnson, W. Chen, M. W. Wong, J. L. Andres, C. Gonzalez, M. Head-Gordon, E. S. Replogle, and J. A. Pople. Gaussian 98, Revision A.7. Gaussian Inc., Pittsburgh, PA, 1998.
[32] A. J. Dyson and P. V. Smith, Mol. Phys. **96**, 1491 (1999).
[33] C. Sbraccia, P. Silvestrelli, and F. Ancilotto, Surf. Sci. **516**, 147 (2002).
[34] K. Blum, *Density Matrix Theory and Applications* (Plenum, New York, 1989).
[35] I. S. Gradshteyn and I. M. Ryzhik, *Table of Integrals, Series, and Products* (Academic, New York, 1980).
[36] W. H. Press, B. P. Flannery, S. A. Teukolsky, and W. T. Vetterling, *Numerical Recipies* (Cambridge University Press, Cambridge, 1986).
[37] M. V. Korolkov, J. Manz, and G. K. Paramonov, J. Phys. Chem. **101**, 13927 (1996).
[38] M. V. Korolkov, J. Manz, and G. K. Paramonov, J. Chem. Phys. **105**, 10874 (1996).
[39] M. V. Korolkov and G. K. Paramonov, Phys. Rev. A **56**, 3860 (1997).
[40] S. Beyvers, Y. Ohtsuki, and P. Saalfrank, J. Chem. Phys. **124**, 234706 (2006).
[41] D. W. Oxtoby, J. Chem. Phys. **70**, 2605 (1979).
[42] P. Saalfrank and R. Kosloff, J. Chem. Phys. **105**, 2441 (1996).
[43] G. K. Paramonov, in *Femtosecond Chemistry*, edited by J. Manz and L. Wöste (Verlag Chemie, Weinheim, 1995), Vol. 2, p. 671.
[44] K. Husimi, Proc. Phys. Math. Soc. Jpn. **22**, 264 (1940).
[45] G. K. Paramonov, I. Andrianov, and P. Saalfrank (unpublished).